

1 **Formation drivers and photochemical effects of ClNO₂ in a coastal city of**
2 **Southeast China**

3 Gaojie Chen^{1,4,5}, Xiaolong Fan^{1,4}, Haichao Wang^{2*}, Yee Jun Tham³, Ziyi Lin^{1,4,5}, Xiaoting Ji^{1,4,5}, Lingling
4 Xu^{1,4}, Baoye Hu⁶, Jinsheng Chen^{1,4*}

5
6 ¹Center for Excellence in Regional Atmospheric Environment, Institute of Urban Environment, Chinese
7 Academy of Sciences, Xiamen 361021, China

8 ²School of Atmospheric Sciences, Sun Yat-sen University, Zhuhai 519082, China

9 ³School of Marine Sciences, Sun Yat-sen University, Zhuhai 519082, China

10 ⁴Fujian Key Laboratory of Atmospheric Ozone Pollution Prevention, Institute of Urban Environment,
11 Chinese Academy of Sciences, Xiamen 361021, China

12 ⁵University of Chinese Academy of Sciences, Beijing 100049, China

13 ⁶Minnan Normal University, Zhangzhou 363000, China

14
15 *Correspondence to: Jinsheng Chen (jschen@iue.ac.cn); Haichao Wang (wanghch27@mail.sysu.edu.cn).
16
17
18
19
20
21
22
23
24
25
26
27
28
29
30

31
32 **Abstract.** Nitryl chloride (ClNO₂) is an important precursor of chlorine (Cl) radical, significantly affecting
33 ozone (O₃) formation and photochemical oxidation. However, the key drivers of ClNO₂ production are not
34 fully understood. In this study, the field observations of ClNO₂ and related parameters were conducted in a
35 coastal city of Southeast China during the autumn of 2022, combining with machine learning and model
36 simulations to elucidate its key influencing factors and atmospheric impacts. Elevated concentrations of
37 ClNO₂ (> 500 ppt) were notably observed during nighttime in late autumn, accompanied by increased levels
38 of dinitrogen pentoxide (N₂O₅) and nitrate (NO₃⁻). Nighttime concentrations of ClNO₂ peaked at 3.4 ppb,
39 while its daytime levels remained significant, reaching up to 100 ppt and sustaining at approximately 40 ppt
40 at noon. Machine learning and field observations identified nighttime N₂O₅ heterogeneous uptake as the
41 predominant pathway for ClNO₂ production, whereas NO₃⁻ photolysis may contributed to its daytime
42 generation. Additionally, ambient temperature (T) and relative humidity (RH) emerged as primary
43 meteorological factors affecting ClNO₂ formation, mainly through their effects on thermal equilibrium and
44 N₂O₅ hydrolysis processes, respectively. Ultraviolet (UV) radiation was found to play a dual role in ClNO₂
45 concentrations around noon. Box model simulations showed that under high ClNO₂ conditions, the rates of
46 alkane oxidation by Cl radical in the early morning exceeded those by OH radical. Consequently, VOC
47 oxidation by Cl radical contributed ~ 19% to RO_x production rates, thereby significantly impacting O₃
48 formation and atmospheric oxidation capacity. This research enriched the understanding of ClNO₂
49 generation and loss pathways, providing valuable insights for the regulation of photochemical pollution in
50 coastal regions.

62

63 **1 Introduction**

64 Chlorine (Cl) radical, as an important atmospheric oxidant, can react with volatile organic compounds
65 (VOCs) to affect RO_x (including OH, HO₂, and RO₂) radicals and ozone (O₃) formation (Yi et al., 2023),
66 thereby perturbing atmospheric chemical components and air quality (Peng et al., 2021; Li et al., 2020). The
67 reaction rates between Cl radical and some alkanes are several orders of magnitude faster than those
68 involving OH radical (Atkinson et al., 2006). Furthermore, the related studies indicated that the production
69 rates of Cl radical in the early morning could significantly exceed the production rates of OH radical formed
70 via O₃ photolysis (Phillips et al., 2012; Tham et al., 2016), thereby enhancing the atmospheric oxidation
71 capacity.

72 Nitryl chloride (ClNO₂) is one of the major Cl radical precursors in the tropospheric atmosphere
73 (Thornton et al., 2010; Xue et al., 2015; Liu et al., 2017). It is mainly generated by the heterogeneous uptake
74 of dinitrogen pentoxide (N₂O₅) on chloride-containing aerosols (Finlayson-Pitts et al., 1989; Thornton et al.,
75 2010), among which N₂O₅ is produced through the equilibrium reaction with nitrogen dioxide (NO₂) and
76 nitrate (NO₃) radical. Since Osthoff et al. (2008) firstly detected over 1 ppb of ClNO₂ in the urban outflows
77 of America (Osthoff et al., 2008), significant production of ClNO₂ has been widely observed in the polluted
78 coastal and inland areas with abundant anthropogenic emissions and chloride sources, with concentrations
79 ranging from tens of ppt to several ppb (Riedel et al., 2012; Mielke et al., 2013; Mielke et al., 2011; Phillips
80 et al., 2012; Bannan et al., 2015; Wang et al., 2016; Xia et al., 2020; Xia et al., 2021; Yun et al., 2018; Wang
81 et al., 2022; Li et al., 2023). For the diurnal profile of ClNO₂, its concentrations generally peaked and
82 accumulated at midnight, then rapidly decreased to low levels due to strong photolysis after sunrise (Ma et
83 al., 2023; Mielke et al., 2011; Xia et al., 2020). However, elevated daytime concentrations of ClNO₂ have
84 been observed in field studies, mainly attributed to reduced photolysis rates under heavy cloud or fog cover,
85 as well as contributions from horizontal and vertical transport (Tham et al., 2016; Xia et al., 2021; Jeong et
86 al., 2019; Mielke et al., 2013; Bannan et al., 2015). Notably, the recent laboratory research demonstrated that
87 nitrate (NO₃⁻) photolysis can generate ClNO₂ alongside Cl₂ (Dalton et al., 2023), yet this mechanism has not
88 been confirmed under real atmospheric conditions.

89 At present, the observation studies of ClNO₂ focused on investigating its influencing factors, such as
90 the N₂O₅ uptake coefficient and the production yield of ClNO₂ (Thornton et al., 2003; Tham et al., 2018).
91 The field and laboratory studies have indicated that ClNO₂ production was mainly affected by ambient
92 temperature (T), relative humidity (RH), and particle components (e.g., chloride (Cl⁻), NO₃⁻, and liquid

93 water content) (Bertram and Thornton, 2009; Wang et al., 2023; Wang et al., 2020). In addition to
94 influencing factors, the photochemical effects of ClNO₂ photolysis have been extensively evaluated (Xue et
95 al., 2015; Xia et al., 2021; Tham et al., 2016). Cl radical released by ClNO₂ photolysis will oxidize VOCs to
96 promote the formation RO₂ radical and O₃, greatly compensating for the underestimation of RO₂ radical and
97 O₃ generation in model simulations (Peng et al., 2021; Ma et al., 2023). The field measurements of ClNO₂
98 have been conducted in different atmospheric environments, while the key drivers of ClNO₂ chemistry were
99 still not well recognized. Moreover, it is pertinent to explore whether there are additional and unrecognized
100 sources of ClNO₂ beyond its heterogeneous generation from N₂O₅.

101 In this study, the comprehensive measurements of ClNO₂ and related parameters were conducted in a
102 coastal city of Southeast China during the autumn of 2022. Field observations, combined with a machine
103 learning model, were used to reveal the key driving factors of ClNO₂ formation. Furthermore, we further
104 investigated the potential mechanisms driving daytime ClNO₂ generation. Additionally, we also assessed the
105 photochemical impacts of ClNO₂ based on a box model. Overall, this study underscored the important role
106 of NO₃⁻ in the ClNO₂ chemistry.

107 **2 Materials and methods**

108 **2.1 Field Measurements**

109 The intensive field measurements of ClNO₂, related precursors, and meteorological parameters from
110 October 9th to December 5th, 2022 were performed at an urban site (Institute of Urban Environment,
111 Chinese Academy of Sciences) in a coastal city (Xiamen) of Southeast China (Fig. S1). Here, ClNO₂, N₂O₅,
112 gaseous pollutants (volatile organic compounds (VOCs), NO_x, SO₂, CO, and O₃), aerosol mass
113 concentrations, ionic components, size distribution, and meteorological factors were simultaneously detected.
114 Meanwhile, an iodide-adduct time-of-flight chemical ionization mass spectrometer (I⁻-ToF-CIMS) was used
115 to measure ClNO₂ and N₂O₅. The principles and settings of I⁻-ToF-CIMS were similar with previous studies
116 (Ma et al., 2023; Yan et al., 2023). Detailed descriptions of this observation site and instruments have been
117 provided in previous work (Chen et al., 2024; Hu et al., 2022), Text S1, and Table S1. For the calibrations of
118 ClNO₂ and N₂O₅, ClNO₂ was produced by passing Cl₂ (6 ppm in N₂) through a moist mixture of sodium
119 nitrite (NaNO₂) and sodium chloride (NaCl) (Thaler et al., 2011; Wang et al., 2022), and N₂O₅ was
120 synthesized by the reactions of O₃ and excessive NO₂ (Tham et al., 2016; Wang et al., 2016). The
121 dependences of ClNO₂ and N₂O₅ sensitivities on relative humidity are presented in Fig. S2. The uncertainties
122 of the ClNO₂ and N₂O₅ measurements were estimated to be ~15 and 12 %, respectively~~~20 %~~. The details of

124 ClNO₂ and N₂O₅ calibrations and uncertainty analysis are displayed in Text S2.

125 **2.2 Machine Learning model**

126 Here, the extreme gradient boosting (XGBoost) model coupling with the Shapely additive explanations
127 (SHAP) model (the XGBoost-SHAP model) was used to identify the key influencing factors of ClNO₂
128 formation. Meanwhile, the XGBoost model was applied to establish the predictive model of ClNO₂ based on
129 the observed data of gaseous precursors and meteorological factors; the SHAP model was employed to
130 evaluate the importance of each feature affecting the simulated concentrations of ClNO₂. The SHAP model
131 is an interpretability tool designed to analyze the contributions of individual features to model predictions. It
132 employs an additive explanatory framework that considers all features as contributors, drawing inspiration
133 from cooperative game theory. For each predicted instance, SHAP assigns a Shapley value, representing the
134 cumulative contribution of each feature. Positive SHAP values indicate that a feature increases the model's
135 predicted outcome, signifying a positive contribution. Conversely, negative SHAP values suggest that the
136 feature reduces the predicted value, reflecting a negative contribution. The absolute value of the SHAP score
137 reflects the magnitude of the contribution, regardless of direction, offering insight into the overall
138 importance of the feature. The true value, on the other hand, reveals the direction of the contribution
139 (positive or negative), facilitating a clearer understanding of the relationship between the feature and the
140 prediction. Besides, the partial dependence plot (PDP) analysis offers a visual representation of the marginal
141 effect that the factors have on the model's predicted outcome. It is based on the principle of stabilizing the
142 values of non-target features, and systematically altered the target feature's values according to the model's
143 algorithmic framework to derive the predicted values.

144 ClNO₂ concentrations served as the dependent variable, with trace gases (SO₂, CO, NO₂, NO, O₃, and
145 N₂O₅), PM_{2.5} and its inorganic compositions (NO₃⁻, SO₄²⁻, NH₄⁺, and Cl⁻), and meteorological parameters (T,
146 RH, UV, WS, WD, and BLH) acting as independent variables. The simulated ClNO₂ concentrations by the
147 XGBoost model were highly similar with the observed values (R²=0.91), indicating the good performance of
148 the XGBoost model (Fig. S3). Detailed introductions and settings of the XGBoost-SHAP model are
149 provided in Text S3.

150 **2.3 The box model**

151 The observation-based model (OBM) was utilized to assess the impacts of ClNO₂ on photochemically
152 atmospheric oxidation. As delineated in earlier studies (Xue et al., 2015; Tham et al., 2016; Xia et al., 2021;
153 Peng et al., 2021; Peng et al., 2022), the Master Chemical Mechanism (MCM, version 3.3.1) was adopted,
154 and established chlorine chemistry mechanisms have been integrated. The Tropospheric Ultraviolet and

Visible Radiation (TUV) model was used to calculate ClNO₂ photolysis rates (*J*ClNO₂) under clear-sky conditions. The simulated *J*ClNO₂ values were then scaled based on field-measured *J*NO₂ values. A thorough exposition of the box model configuration can be found in our previous publications (Liu et al., 2022b; Liu et al., 2022a) and Text S4. Observation data, including ClNO₂, VOCs, HCHO, HONO, CO, O₃, NO, NO₂, SO₂, along with meteorological factors as constraint were input into the box model at an hourly resolution (Table S2). ~~Due to the levels of ClNO₂ in the box model determined by observed levels of ClNO₂, the parametrization for N₂O₅ uptake and ClNO₂ yield was not utilized in the box model.~~ Two scenarios were examined: one representing observation-average conditions from October 9th to December 5th, the other reflecting a high ClNO₂ case observed on November 28th.

This study focused on elucidating the influence of ClNO₂ on the formation of RO_x radical and O₃. The O₃ production rate minus the O₃ loss rate was used to calculate the net O₃ production rate (Eq. S1-3). The AOC is calculated by the sum of the rates of CH₄, CO, and VOCs oxidized by atmospheric oxidants (O₃, OH, Cl, and NO₃ radical) (Eq. S4) (Xue et al., 2015; Yi et al., 2023). Both scenarios were evaluated with and without including ClNO₂ inputs to assess its impacts on these processes.

3 Results and discussion

3.1 Overview of observations

Fig. 1 displays the time series of ClNO₂, N₂O₅, and related parameters including O₃, NO_x, PM_{2.5}, Cl⁻, NO₃⁻, and meteorological parameters during the autumn observation period. Our observation shows a decline in T and UV values from October to November, with average RH values increasing from ~ 60% in October to ~ 70% in November (excluding rainy days). During the entire measurement period, ClNO₂ concentrations exhibited significant variability, with elevated levels (> 500 ppt) frequently observed in late autumn, particularly after November 10th. The elevation of ClNO₂ concentrations coincided with increased levels of N₂O₅ and NO₃⁻ during late autumn. The concentrations of ClNO₂ at our study site reached several ppb, compared with previous field measurements conducted at urban, suburban, rural, background, and mountain sites (Table S3), indicating its widespread presence in diverse atmospheric environments. The highest concentrations of ClNO₂ were detected during the night of November 27th, with a maximum hourly average of 3.4 ppb. Peak concentrations of N₂O₅ and NO₃⁻ were also observed on that night (Fig. 1). On the evening of November 27th, N₂O₅ concentrations rapidly decreased after 7 p.m., while ClNO₂ and NO₃⁻ concentrations significantly increased, reflecting fast N₂O₅ heterogeneous hydrolysis and effective formation of ClNO₂. Notably, on the following day (November 28th) (Fig. 2a), ClNO₂ concentrations sustained above

100 ppt around noon, partially related with weakened UV values ($\sim 14 \text{ W}\cdot\text{m}^{-2}$) under heavy fog and cloud cover, with the RH values of $\sim 70\%$ at that time. Similar research in California has shown ClNO_2 concentrations exceeding 100 ppt after sunrise 4 hours due to reduced photolysis (Mielke et al., 2013).

The average diurnal changes of ClNO_2 and related parameters during the entire measurement campaign are depicted in Fig. 2b. As expected, ClNO_2 exhibited a distinct diurnal variation, peaking and accumulating after sunset and decreasing in the early morning. However, ClNO_2 concentrations remained ~ 40 ppt around noon, different with some studies that ClNO_2 concentrations decreased to near the detection limit around midday (Wang et al., 2022; Niu et al., 2022). Similar observation in North China declared ClNO_2 concentrations above 60 ppt in the afternoon (Liu et al., 2017). Previous studies have indicated that abundant ClNO_2 may be transported from upper atmosphere or air mass, contributing to the elevated ClNO_2 concentrations in the early morning (Tham et al., 2016; Xia et al., 2021; Jeong et al., 2019). However, the explanations for the concentrations of ClNO_2 around noon remained elusive.

To evaluate the contribution of the heterogeneous N_2O_5 uptake to daytime ClNO_2 levels, we calculated ClNO_2 production using a box model, considering (1) the contribution of heterogeneous N_2O_5 uptake to ClNO_2 production, and (2) ClNO_2 loss via photolysis, aerosol uptake, and reaction with $\text{OH}\cdot$ (Text S5 and S6). We used a $\gamma(\text{N}_2\text{O}_5)$ value of 0.06, a $\phi(\text{ClNO}_2)$ value of 1.0, and a $\gamma(\text{ClNO}_2)$ value of 0.006 in our calculations, which represent upper-end estimates based on previous field studies (Mcduffie et al., 2018a; Mcduffie et al., 2018b; Tham et al., 2016). However, as shown in Fig. 3, the simulated daytime ClNO_2 concentrations were lower than the observed values. Therefore, we believe that the observed daytime ClNO_2 levels, particularly around noon, cannot be adequately explained by heterogeneous N_2O_5 uptake alone, suggesting the presence of additional sources contributing to the formation of daytime ClNO_2 .

~~To evaluate the contribution of the heterogeneous N_2O_5 uptake to daytime ClNO_2 levels, we calculated ClNO_2 production using Eq. (S7), considering the loss of ClNO_2 through photolysis. This method has been employed in a previous study (Text S4 S5) (Tham et al., 2016). We used a $\gamma(\text{N}_2\text{O}_5)$ value of 0.06 and a $\phi(\text{ClNO}_2)$ value of 1.0 in our calculations, which represent upper-end estimates based on previous field studies (Meduffie et al., 2018a; Meduffie et al., 2018b; Tham et al., 2016). However, as shown in Fig. 3, the calculated $\phi(\text{ClNO}_2)$ with $\gamma(\text{N}_2\text{O}_5) = 0.06$ fails to reproduce the observed levels of daytime ClNO_2 . A larger $\gamma(\text{N}_2\text{O}_5)$ of 0.11 would be necessary, but such high uptake coefficients and yields are not supported by the current literature. Therefore, we believe that the observed daytime ClNO_2 levels, particularly around noon, cannot be adequately explained by heterogeneous N_2O_5 uptake alone, suggesting the presence of additional sources contributing to the formation of daytime ClNO_2 .~~

217

218 **3.2 Key drivers of ClNO₂ formation**

219 The XGBoost-SHAP model was employed to investigate the major drivers of ClNO₂ production during
220 the whole observation period. The average absolute SHAP value of each feature was ranked to determine the
221 key drivers of ClNO₂ formation, with larger SHAP values suggesting greater contributions (Fig. 4a).
222 Additionally, features with positive SHAP values (depicted as red points) indicate that higher values of those
223 features positively affect ClNO₂ concentrations, and vice versa (Fig. 4b). Overall, N₂O₅, NO₃⁻, T, RH, and
224 UV were the most important features affecting ClNO₂ concentrations. Notably, these factors exhibited varied
225 behaviors between daytime and nighttime periods.

226 In our study, N₂O₅ was identified as the most important influencing factor, consistent with its role in
227 ClNO₂ formation through heterogeneous uptake processes (Thornton et al., 2010; Finlayson-Pitts et al.,
228 1989). After sunset, ClNO₂ concentrations markedly increased due to active nighttime N₂O₅ chemistry,
229 while this heterogeneous uptake process was hindered after sunrise as N₂O₅ concentrations decreased
230 significantly (Fig. 1) (Niu et al., 2022; Wang et al., 2020; Tan et al., 2022). Indeed, the concentrations of
231 ClNO₂ were evidently increased when N₂O₅ concentrations exceeded ~13 ppt, predominantly during the
232 nighttime (Fig. 5a). Conversely, in Northern Europe, the ClNO₂ concentrations were mainly controlled by
233 O₃ and NO₂, rather than by the heterogeneous uptake of N₂O₅ (Sommariva et al., 2018). In Heshan of South
234 China, chloride and PM_{2.5} were the major factors affecting ClNO₂ formation (Wang et al., 2022). Differently,
235 the relative importance of NO₃⁻ derived from the XGBoost-SHAP result indicated that elevated ClNO₂
236 concentrations were associated with high concentrations of NO₃⁻ besides N₂O₅. According to Fig. 5b, high
237 NO₃⁻ concentrations (> 3.7 μg·m⁻³) are accompanied by the elevation of ClNO₂, especially its
238 concentrations reaching 6.2 μg·m⁻³. Previous studies suggested that increased concentrations of NO₃⁻
239 decreased γ(N₂O₅), which would limit the production of ClNO₂ (Wahner et al., 1998; Mentel et al., 1999;
240 Bertram and Thornton, 2009). As depicted in Fig. S4, the dependence of γ(N₂O₅) on NO₃⁻ concentrations
241 follows the nitrate suppression effect. Therefore, the importance of nighttime NO₃⁻ for ClNO₂ levels is that
242 they are co-products from the processes of N₂O₅ heterogeneous uptake. As shown in Fig. 1, compared to low
243 NO₃⁻ conditions, ClNO₂ production was enhanced in high NO₃⁻ conditions. Especially in late autumn,
244 increased aerosol abundances and N₂O₅ levels increased N₂O₅ uptake further promoting ClNO₂ and
245 NO₃⁻ production. Considering the limited contribution of N₂O₅ hydrolysis to daytime NO₃⁻ levels (Yan et al.,
246 2023; Zang et al., 2022; Chen et al., 2020), the impact of high NO₃⁻ concentrations on daytime ClNO₂
247 concentrations warrants further analysis.

The simulated concentrations of ClNO₂, based on the XGBoost-SHAP model, were significantly elevated when NO₃⁻ concentrations were higher than 3.7 μg·m⁻³ (Fig. 5b). Consequently, the average daily concentrations of NO₃⁻ were classified as high (> 3.7 μg·m⁻³) and low (< 3.7 μg·m⁻³) to further elucidate the impacts of NO₃⁻ on the formation of ClNO₂. Fig. 6 presents the diurnal variations in the relative importance of factors based on the SHAP values under high and low NO₃⁻ concentrations. Unexpectedly, daytime NO₃⁻ was the dominant influencing factors for daytime ClNO₂ (Fig. 6a). High concentrations of daytime NO₃⁻ positively affected the daytime concentrations of ClNO₂, independent of N₂O₅ uptake processes. As depicted in Fig. 6a, daytime N₂O₅ did not promote the elevation of daytime ClNO₂. Negative SHAP values for N₂O₅ during the daytime indicate that the contribution of N₂O₅ chemistry to daytime ClNO₂ levels was limited. Therefore, it is very likely that high concentrations of daytime NO₃⁻ participated in daytime ClNO₂ production. A recent study suggested that nitrate photolysis produced ClNO₂ in addition to Cl₂ (Dalton et al., 2023), while it has been not verified by field observations. Fig. 7 shows that daytime ClNO₂ concentrations correlated well (R=0.62) with the product of a proxy of NO₃⁻ photolysis (NO₃⁻×JNO₂×S_a) on aerosol surfaces—(S_a), implying that the photolysis of NO₃⁻ likely resulted in the daytime formation of ClNO₂ contributed to the daytime concentrations of ClNO₂ at our study site. Furthermore, high concentrations of NO₃⁻ and Cl⁻, along with large values of S_a (Fig. 7a, b, c and Fig. S5) in the daytime accelerated NO₃⁻ photolysis, promoting the formation of ClNO₂, while ClNO₂ concentrations exhibited a weak correlation with JNO₂. It should be emphasized that the weak correlation between JNO₂ and ClNO₂ concentrations does not deny the potential contribution of nitrate photolysis, which could be explained by the fact that ClNO₂ concentrations are affected by both its production and loss processes. Specifically, photolysis rates exert dual effects on daytime ClNO₂ concentrations: positive effects through photochemical production pathways and negative effects through direct ClNO₂ photolytic loss. Given the short daytime lifetime of ClNO₂, we calculated the missing ClNO₂ production rate (production rate minus loss rate) to assess the contributions from unknown sources (Text S6). The production rate of unknown source showed a good correlation with JNO₂ (R=0.41) (Fig. S6), indicating that photochemical processes may enhance ClNO₂ production. Notably, the strong correlation between the observed concentrations of ClNO₂ and the NO₃⁻ photolysis proxy (NO₃⁻×JNO₂×S_a) has revealed the possibility of the contribution of NO₃⁻ photolysis to the unknown daytime ClNO₂ source. ~~Overall, N₂O₅ uptake processes were the major pathways dominating nighttime ClNO₂ formation, while NO₃⁻ photolysis contributed to daytime ClNO₂ production during our observation period.~~

In term of meteorological factors, UV, T, and RH were the major influencing factors. The photolysis

279 was the most important sink of ClNO₂ in the daytime, leading to a rapid reduction in ClNO₂ concentrations,
280 particularly in the early morning (Fig. 5e and Fig. 6). However, it is crucial to understand the dual role of
281 photolysis intensity in determining daytime ClNO₂ levels. As mentioned before, photolysis can contribute
282 to the generation of ClNO₂ by promoting NO₃⁻ photolysis, while also causing the rapid decomposition of
283 ClNO₂. As reported in California (Mielke et al., 2013), reduced photolysis rates even increased daytime
284 ClNO₂ levels by decreasing ClNO₂ loss through photolysis. The impact of ambient temperature on ClNO₂
285 was probably reflected in its thermal equilibrium with N₂O₅. Elevated daytime ambient temperature
286 suppressed the formation of N₂O₅, resulting in low N₂O₅ concentrations, which further limited the
287 contribution of heterogeneous N₂O₅ uptake to daytime ClNO₂ generation (Fig. 5c and Fig. 6). During the
288 whole observation period from October to November, the drop in ambient temperature facilitated ClNO₂
289 production by decreasing the thermal decomposition process. Increased RH values provided favorable
290 conditions for the nighttime N₂O₅ hydrolysis reactions, thereby affecting ClNO₂ production (Fig. 5d and Fig.
291 6), while high RH (> 80%) also weakened the generation of ClNO₂. Notably, Cl⁻ was not the most important
292 factors of ClNO₂ formation at our study site (Fig. 4), likely attributed to the abundant chlorine source in
293 coastal regions (Peng et al., 2022).

294 **3.3 Impact of ClNO₂ photolysis on RO_x budget**

295 The photochemical effects of ClNO₂ were evaluated under the observation-average condition and the
296 high ClNO₂ case based on the box model. The largest Cl production rates (P(Cl)) contributed from ClNO₂
297 photolysis were 0.05 ppb·h⁻¹ for the observation-average condition, which was lower than 0.19 ppb·h⁻¹ for
298 the high ClNO₂ case. The difference led to variable levels of atmospheric oxidation capacity induced by Cl
299 radical. Cl radical released via the photolysis of ClNO₂ initiated the oxidation of VOCs. Among VOC
300 groups (including alkanes, alkenes, alkynes, aromatics and OVOCs), Cl radical primarily oxidized alkanes
301 (~ 65.0%), followed by OVOCs (~ 12.7%) for both the observation-average condition and the high ClNO₂
302 case (Fig. 8a, b). The contributions of Cl radical and other atmospheric oxidants (including OH radical and
303 O₃) to daytime VOC oxidation were also compared (Fig. 8c, d and Table 1). In our study, the oxidation of
304 alkanes by Cl radical for the observation-average condition were about 11.7%, which increased by 44.8%
305 for the high ClNO₂ case, were higher than those in London (Bannan et al., 2015), Weybourne (Bannan et al.,
306 2017), Boston (Rutherford et al., 1995), and LA (Fraser et al., 1997), lower than that in Hong Kong (Xue et
307 al., 2015). It should be noticed that the rates of Cl radical reacting with alkanes even exceeded those of OH
308 radical in the early morning for the high ClNO₂ case. The largest rates of alkanes oxidized by Cl radical were
309 approximately twice as high as those of OH radical at 10 a.m. (Fig. 8e, f), highlighting that the

310 photochemical effects of Cl radical released via ClNO₂ photolysis were particularly important for VOC
311 oxidation during the morning hours at our study site.

312 The oxidation of VOCs by Cl radical further affects the generation of RO_x (OH + HO₂ + RO₂) radicals.
313 The RO_x radical production rates for the high ClNO₂ case were evidently lower than that under the
314 observation-average condition, primarily due to reduced photolysis rates on that day. However, the total RO_x
315 radical production rates averagely increased by 23.8% with ClNO₂ photolysis for the high ClNO₂ case,
316 higher than a 4.9% increase for the observation-average condition (Fig. S5S7). For the observation-average
317 condition, O₃ (32.7%), HONO (31.7%), and OVOCs (21.6%) photolysis were the most significant
318 contributors to RO_x radical production in the early morning (7-10 a.m.), with VOC oxidation by Cl radical
319 contributing only 3.7% (Fig. 9a). However, for the high ClNO₂ case, VOC oxidation induced by Cl radical
320 in the early morning accounted for 19.1% of RO_x radical production, which was higher than O₃ (7.4%) and
321 HCHO (4.1%) photolysis, close to OVOCs (19.0%) photolysis (Fig. 9b). The contributions of ClNO₂
322 photolysis to the RO_x radical production rates in our study were larger than previous results observed in
323 autumn of Heshan (Wang et al., 2022) and North China (Xia et al., 2021), similar with that in summer of
324 Wangdu (Tham et al., 2016). Thus, the concentrations of OH, HO₂, and RO₂ radicals in the box model with
325 ClNO₂ inputs averagely increased by 17.9%, 34.6%, and 54.3% for the high ClNO₂ case, higher than the
326 increases of 3.7%, 7.1%, and 10.3% contributed from the observation-average conditions, respectively (Fig.
327 S6S8). The uplift in the concentrations of RO_x radicals also accelerated the generation of O₃. The increase in
328 the net O₃ production rates (P(O₃)) for the observation-average condition averagely reached 0.13 ppb·h⁻¹
329 (15.8 %) in the daytime (Fig. 10a), while larger elevations in the net P(O₃) were observed for the high
330 ClNO₂ case (Fig. 10b), with a maximum of 0.64 ppb·h⁻¹ (120 %) at 10 a.m. As a result, increased RO_x
331 radical and O₃ greatly enhanced the atmospheric oxidation capacity (Fig. 10c, d), especially for the high
332 ClNO₂ case (up to 65%).

333 Table 2 summarizes the impacts of ClNO₂ photolysis on RO_x radical and O₃ production in our study
334 and previous observations around the world (Xia et al., 2021; Wang et al., 2022; Tham et al., 2016; Wang et
335 al., 2016; Xue et al., 2015; Bannan et al., 2017; Jeong et al., 2019), indicating that the photochemical
336 impacts of ClNO₂ were variable in different atmospheric environments. At our study site, the effects of
337 ClNO₂ photolysis on RO_x radical production were important, especially in the early morning. The enhanced
338 RO_x radical production induced by ClNO₂ photolysis accelerated the chemical generation of O₃. Primary
339 RO_x radical production rates (including O₃, HONO, HCHO, OVOCs, and ClNO₂) were considered as one of
340 the most important parameters to O₃ formation (Lu et al., 2023). Therefore, the considerable contribution of

341 ClNO₂ photolysis to primary RO_x radical production in the early morning may bring new challenges for O₃
342 alleviation.

344 **Conclusions**

345 In conclusion, we present two months of field measurements in the coastal area of Southern China
346 during the autumn, coupled with machine learning and model simulations, providing new insights into
347 ClNO₂ chemistry. Our observation shows the increase in the concentrations of ClNO₂ were accompanied by
348 elevated concentrations of N₂O₅ and NO₃⁻, low values of T and UV, and high values of RH. The nighttime
349 heterogeneous uptake of N₂O₅ was identified as the major source of ClNO₂, while NO₃⁻ photolysis served as
350 a potential daytime ClNO₂ source~~NO₃⁻ photolysis promoted the elevation of daytime ClNO₂ concentrations.~~
351 Cl radical released by ClNO₂ photolysis after sunrise had important photochemical effects in the early
352 morning. The photolysis of high ClNO₂ concentrations resulted in net O₃ production rates and atmospheric
353 oxidation capacity levels increasing by 120% and 65%, respectively. Our results enhanced the understanding
354 of ClNO₂ chemistry in coastal regions, calling for more observations and laboratory research to fully reveal
355 its exact role in different atmospheric environments.

356
357 **Data availability.** Data are available upon request to Jinsheng Chen (jschen@iue.ac.cn).

358
359 **Author contributions.** JC provided funding support for field measurements, designed this study, and
360 revised this manuscript. GC designed this study, analyzed the data, and wrote this manuscript. HW helped
361 perform the calibrations and revised this manuscript. XF revised this manuscript. XF, HW, YT, ZL, XJ, LX,
362 BH contributed to discussions of this manuscript.

363
364 **Competing interests.** The authors declare that they have no conflict of interest.

365
366 **Acknowledgements.** The authors acknowledge the National Natural Science Foundation of China, the
367 Science and Technology Department of Fujian Province, Center for Excellence in Regional Atmospheric
368 Environment Project, Xiamen Atmospheric Environment Observation and Research Station of Fujian
369 Province, and Fujian Key Laboratory of Atmospheric Ozone Pollution Prevention (Institute of Urban
370 Environment, Chinese Academy of Sciences).

372 **Financial support.** This work was funded by the National Natural Science Foundation of China
373 (U22A20578, 42305102 & 42277091), the Science and Technology Department of Fujian Province
374 (2022L3025), the National Key Research and Development Program (2022YFC3700304), STS Plan
375 Supporting Project of the Chinese Academy of Sciences in Fujian Province (2023T3013), Fujian Provincial
376 Environmental Protection Science & Technology Plan Projects (2023R004), and Xiamen Atmospheric
377 Environment Observation and Research Station of Fujian Province. Y.J.T. acknowledges the funding support
378 from the Guangdong Basic and Applied Basic Research Foundation (2022A1515010852) and the
379 Fundamental Research Funds for the Central Universities, Sun Yat-sen University (23hytd002).

381 **References**

382 Atkinson, R., Baulch, D. L., Cox, R. A., Crowley, J. N., Hampson, R. F., Hynes, R. G., Jenkin, M. E., Rossi,
383 M. J., Troe, J., and Subcommittee, I.: Evaluated kinetic and photochemical data for atmospheric chemistry:
384 Volume II – gas phase reactions of organic species, *Atmos. Chem. Phys.*, 6, 3625-4055,
385 <https://doi.org/10.5194/acp-6-3625-2006>, 2006.

386 Bannan, T. J., Bacak, A., Le Breton, M., Flynn, M., Ouyang, B., McLeod, M., Jones, R., Malkin, T. L.,
387 Whalley, L. K., Heard, D. E., Bandy, B., Khan, M. A. H., Shallcross, D. E., and Percival, C. J.: Ground and
388 Airborne U.K. Measurements of Nitryl Chloride: An Investigation of the Role of Cl Atom Oxidation at
389 Weybourne Atmospheric Observatory, *J. Geophys. Res. Atmos.*, 122, 111,154-111,165,
390 <https://doi.org/10.1002/2017jd026624>, 2017.

391 Bannan, T. J., Booth, A. M., Bacak, A., Muller, J. B. A., Leather, K. E., Le Breton, M., Jones, B., Young, D.,
392 Coe, H., Allan, J., Visser, S., Slowik, J. G., Furger, M., Prévôt, A. S. H., Lee, J., Dunmore, R. E., Hopkins, J.
393 R., Hamilton, J. F., Lewis, A. C., Whalley, L. K., Sharp, T., Stone, D., Heard, D. E., Fleming, Z. L., Leigh,
394 R., Shallcross, D. E., and Percival, C. J.: The first UK measurements of nitryl chloride using a chemical
395 ionization mass spectrometer in central London in the summer of 2012, and an investigation of the role of Cl
396 atom oxidation, *J. Geophys. Res. Atmos.*, 120, 5638-5657, <https://doi.org/10.1002/2014jd022629>, 2015.

397 Bertram, T. and Thornton, J.: Toward a general parameterization of N₂O₅ reactivity on aqueous particles: the
398 competing effects of particle liquid water, nitrate and chloride, *Atmos. Chem. Phys.*, 9, 8351-8363,
399 <https://doi.org/10.5194/acp-9-8351-2009>, 2009.

400 Chen, G., Ji, X., Chen, J., Xu, L., Hu, B., Lin, Z., Fan, X., Li, M., Hong, Y., and Chen, J.: Photochemical

401 pollution during summertime in a coastal city of Southeast China: Ozone formation and influencing factors,
402 Atmos. Res., 301, 107270, <https://doi.org/10.1016/j.atmosres.2024.107270>, 2024.

403 Chen, X., Wang, H., Lu, K., Li, C., Zhai, T., Tan, Z., Ma, X., Yang, X., Liu, Y., Chen, S., Dong, H., Li, X.,
404 Wu, Z., Hu, M., Zeng, L., and Zhang, Y.: Field Determination of Nitrate Formation Pathway in Winter
405 Beijing, Environ. Sci. Technol., 54, 9243-9253, <https://doi.org/10.1021/acs.est.0c00972>, 2020.

406 Dalton, E. Z., Hoffmann, E. H., Schaefer, T., Tilgner, A., Herrmann, H., and Raff, J. D.: Daytime
407 Atmospheric Halogen Cycling through Aqueous-Phase Oxygen Atom Chemistry, J. Am. Chem. Soc., 145,
408 15652-15657, <https://doi.org/10.1021/jacs.3c03112>, 2023.

409 Finlayson-Pitts, B. J., Ezell, M. J., and Pitts, J. N.: Formation of chemically active chlorine compounds by
410 reactions of atmospheric NaCl particles with gaseous N₂O₅ and ClONO₂, Nature., 337, 241-244,
411 <https://doi.org/10.1038/337241a0>, 1989.

412 Fraser, M. P., Cass, G. R., Simoneit, B. R., and Rasmussen, R.: Air quality model evaluation data for
413 organics. 4. C₂–C₃₆ non-aromatic hydrocarbons, Environ. Sci. Technol., 31, 2356-2367,
414 <https://doi.org/10.1021/es960980g>, 1997.

415 Hu, B., Duan, J., Hong, Y., Xu, L., Li, M., Bian, Y., Qin, M., Fang, W., Xie, P., and Chen, J.: Exploration of
416 the atmospheric chemistry of nitrous acid in a coastal city of southeastern China: results from measurements
417 across four seasons, Atmos. Chem. Phys., 22, 371-393, <https://doi.org/10.5194/acp-22-371-2022>, 2022.

418 Jeong, D., Seco, R., Gu, D., Lee, Y., Nault, B. A., Knote, C. J., McGee, T., Sullivan, J. T., Jimenez, J. L.,
419 Campuzano-Jost, P., Blake, D. R., Sanchez, D., Guenther, A. B., Tanner, D., Huey, L. G., Long, R.,
420 Anderson, B. E., Hall, S. R., Ullmann, K., Shin, H., Herndon, S. C., Lee, Y., Kim, D., Ahn, J., and Kim, S.:
421 Integration of airborne and ground observations of nitryl chloride in the Seoul metropolitan area and the
422 implications on regional oxidation capacity during KORUS-AQ 2016, Atmos. Chem. Phys., 19, 12779-
423 12795, <https://doi.org/10.5194/acp-19-12779-2019>, 2019.

424 Li, F., Huang, D. D., Nie, W., Tham, Y. J., Lou, S., Li, Y., Tian, L., Liu, Y., Zhou, M., and Wang, H.:
425 Observation of nitrogen oxide-influenced chlorine chemistry and source analysis of Cl₂ in the Yangtze River
426 Delta, China, Atmos. Environ., 306, 119829, <https://doi.org/10.1016/j.atmosenv.2023.119829>, 2023.

427 Li, Q., Badia, A., Wang, T., Sarwar, G., Fu, X., Zhang, L., Zhang, Q., Fung, J., Cuevas, C. A., Wang, S.,

428 Zhou, B., and Saiz-Lopez, A.: Potential Effect of Halogens on Atmospheric Oxidation and Air Quality in
429 China, *J. Geophys. Res. Atmos.*, 125, e2019JD032058, <https://doi.org/10.1029/2019JD032058>, 2020.

430 Liu, T., Chen, G., Chen, J., Xu, L., Li, M., Hong, Y., Chen, Y., Ji, X., Yang, C., Chen, Y., Huang, W., Huang,
431 Q., and Wang, H.: Seasonal characteristics of atmospheric peroxyacetyl nitrate (PAN) in a coastal city of
432 Southeast China: Explanatory factors and photochemical effects, *Atmos. Chem. Phys.*, 22, 4339-4353,
433 <https://doi.org/10.5194/acp-22-4339-2022>, 2022a.

434 Liu, T., Hong, Y., Li, M., Xu, L., Chen, J., Bian, Y., Yang, C., Dan, Y., Zhang, Y., Xue, L., Zhao, M., Huang,
435 Z., and Wang, H.: Atmospheric oxidation capacity and ozone pollution mechanism in a coastal city of
436 southeastern China: analysis of a typical photochemical episode by an observation-based model, *Atmos.*
437 *Chem. Phys.*, 22, 2173-2190, <https://doi.org/10.5194/acp-22-2173-2022>, 2022b.

438 Liu, X., Qu, H., Huey, L. G., Wang, Y., Sjostedt, S., Zeng, L., Lu, K., Wu, Y., Hu, M., Shao, M., Zhu, T., and
439 Zhang, Y.: High Levels of Daytime Molecular Chlorine and Nitryl Chloride at a Rural Site on the North
440 China Plain, *Environ. Sci. Technol.*, 51, 9588-9595, <https://doi.org/10.1021/acs.est.7b03039>, 2017.

441 Lu, K., Zhou, H., Lee, J., Nelson, B., and Zhang, Y.: Ozone mitigations beyond the control of nitrogen
442 oxides and volatile organic compounds, *Sci Bull*, 68, 1989-1992, <https://doi.org/10.1016/j.scib.2023.07.051>,
443 2023.

444 Ma, W., Chen, X., Xia, M., Liu, Y., Wang, Y., Zhang, Y., Zheng, F., Zhan, J., Hua, C., and Wang, Z.:
445 Reactive Chlorine Species Advancing the Atmospheric Oxidation Capacities of Inland Urban Environments,
446 *Environ. Sci. Technol.*, 57, 14638-14647, <https://doi.org/10.1021/acs.est.3c05169>, 2023.

447 McDuffie, E. E., Fibiger, D. L., Dubé, W. P., Lopez Hilfiker, F., Lee, B. H., Jaeglé, L., Guo, H., Weber, R. J.,
448 Reeves, J. M., Weinheimer, A. J., Schroder, J. C., Campuzano-Jost, P., Jimenez, J. L., Dibb, J. E., Veres, P.,
449 Ebben, C., Sparks, T. L., Wooldridge, P. J., Cohen, R. C., Campos, T., Hall, S. R., Ullmann, K., Roberts, J.
450 M., Thornton, J. A., and Brown, S. S.: ClNO₂ Yields From Aircraft Measurements During the 2015
451 WINTER Campaign and Critical Evaluation of the Current Parameterization, *J. Geophys. Res. Atmos.*, 123,
452 12,994-913,015, <https://doi.org/10.1029/2018JD029358>, 2018a.

453 McDuffie, E. E., Fibiger, D. L., Dubé, W. P., Lopez-Hilfiker, F., Lee, B. H., Thornton, J. A., Shah, V., Jaeglé,
454 L., Guo, H., Weber, R. J., Michael Reeves, J., Weinheimer, A. J., Schroder, J. C., Campuzano-Jost, P.,

455 Jimenez, J. L., Dibb, J. E., Veres, P., Ebben, C., Sparks, T. L., Wooldridge, P. J., Cohen, R. C., Hornbrook, R.
456 S., Apel, E. C., Campos, T., Hall, S. R., Ullmann, K., and Brown, S. S.: Heterogeneous N₂O₅ Uptake During
457 Winter: Aircraft Measurements During the 2015 WINTER Campaign and Critical Evaluation of Current
458 Parameterizations, *J. Geophys. Res. Atmos.*, 123, 4345-4372, <https://doi.org/10.1002/2018JD028336>, 2018b.

459 Mentel, T. F., Sohn, M., and Wahner, A. J. P. C. C. P.: Nitrate effect in the heterogeneous hydrolysis of
460 dinitrogen pentoxide on aqueous aerosols, *Phys. Chem. Chem. Phys.*, 1, 5451-5457,
461 <https://doi.org/10.1039/A905338g>, 1999.

462 Mielke, L. H., Furgeson, A., and Osthoff, H. D.: Observation of ClNO₂ in a Mid-Continental Urban
463 Environment, *Environ. Sci. Technol.*, 45, 8889-8896, <https://doi.org/10.1021/es201955u>, 2011.

464 Mielke, L. H., Stutz, J., Tsai, C., Hurlock, S. C., Roberts, J. M., Veres, P. R., Froyd, K. D., Hayes, P. L.,
465 Cubison, M. J., Jimenez, J. L., Washenfelder, R. A., Young, C. J., Gilman, J. B., Gouw, J. A., Flynn, J. H.,
466 Grossberg, N., Lefer, B. L., Liu, J., Weber, R. J., and Osthoff, H. D.: Heterogeneous formation of nitryl
467 chloride and its role as a nocturnal NO_x reservoir species during CalNex-LA 2010, *J. Geophys. Res. Atmos.*,
468 118, 10,638-610,652, <https://doi.org/10.1002/jgrd.50783>, 2013.

469 Niu, Y.-B., Zhu, B., He, L.-Y., Wang, Z., Lin, X.-Y., Tang, M.-X., and Huang, X.-F.: Fast Nocturnal
470 Heterogeneous Chemistry in a Coastal Background Atmosphere and Its Implications for Daytime
471 Photochemistry, *J. Geophys. Res. Atmos.*, 127, e2022JD036716, <https://doi.org/10.1029/2022JD036716>,
472 2022.

473 Osthoff, H. D., Roberts, J. M., Ravishankara, A. R., Williams, E. J., Lerner, B. M., Sommariva, R., Bates, T.
474 S., Coffman, D., Quinn, P. K., Dibb, J. E., Stark, H., Burkholder, J. B., Talukdar, R. K., Meagher, J.,
475 Fehsenfeld, F. C., and Brown, S. S.: High levels of nitryl chloride in the polluted subtropical marine
476 boundary layer, *Nat. Geosci.*, 1, 324-328, <https://doi.org/10.1038/ngeo177>, 2008.

477 Peng, X., Wang, T., Wang, W., Ravishankara, A., George, C., Xia, M., Cai, M., Li, Q., Salvador, C. M., and
478 Lau, C.: Photodissociation of particulate nitrate as a source of daytime tropospheric Cl₂, *Nat. Commun.*, 13,
479 1-10, <https://doi.org/10.1038/s41467-022-28383-9>, 2022.

480 Peng, X., Wang, W., Xia, M., Chen, H., Ravishankara, A. R., Li, Q., Saiz-Lopez, A., Liu, P., Zhang, F.,
481 Zhang, C., Xue, L., Wang, X., George, C., Wang, J., Mu, Y., Chen, J., and Wang, T.: An unexpected large

482 continental source of reactive bromine and chlorine with significant impact on wintertime air quality, *Natl.*
483 *Sci. Rev.*, 8, nwaa304, <https://doi.org/10.1093/nsr/nwaa304>, 2021.

484 Phillips, G. J., Tang, M. J., Thieser, J., Brickwedde, B., Schuster, G., Bohn, B., Lelieveld, J., and Crowley, J.
485 N.: Significant concentrations of nitryl chloride observed in rural continental Europe associated with the
486 influence of sea salt chloride and anthropogenic emissions, *Geophys. Res. Lett.*, 39, L10811,
487 <https://doi.org/10.1029/2012gl051912>, 2012.

488 Riedel, T. P., Bertram, T. H., Crisp, T. A., Williams, E. J., Lerner, B. M., Vlasenko, A., Li, S. M., Gilman, J.,
489 de Gouw, J., Bon, D. M., Wagner, N. L., Brown, S. S., and Thornton, J. A.: Nitryl chloride and molecular
490 chlorine in the coastal marine boundary layer, *Environ. Sci. Technol.*, 46, 10463-10470,
491 <https://doi.org/10.1021/es204632r>, 2012.

492 Rutherford, J. A., Koehl, W. J., Benson, J. D., Burns, V. R., Hochhauser, A. M., Knepper, J. C., Leppard, W.
493 R., Painter, L. J., Rapp, L. A., and Rippon, B.: Effects of Gasoline Properties on Emissions of Current and
494 Future Vehicles-T50, T90, and Sulfur Effects-Auto/Oil Air Quality Improvement Research Program, SAE
495 Technical Paper0148-7191, <https://doi.org/10.4271/952510>, 1995.

496 Sommariva, R., Hollis, L. D. J., Sherwen, T., Baker, A. R., Ball, S. M., Bandy, B. J., Bell, T. G., Chowdhury,
497 M. N., Cordell, R. L., Evans, M. J., Lee, J. D., Reed, C., Reeves, C. E., Roberts, J. M., Yang, M., and Monks,
498 P. S.: Seasonal and geographical variability of nitryl chloride and its precursors in Northern Europe, *Atmos.*
499 *Sci. Lett.*, 19, <https://doi.org/10.1002/asl.844>, 2018.

500 Tan, Z., Fuchs, H., Hofzumahaus, A., Bloss, W. J., Bohn, B., Cho, C., Hohaus, T., Holland, F., Lakshmisha,
501 C., Liu, L., Monks, P. S., Novelli, A., Niether, D., Rohrer, F., Tillmann, R., Valkenburg, T. S. E., Vardhan, V.,
502 Kiendler-Scharr, A., Wahner, A., and Sommariva, R.: Seasonal variation in nitryl chloride and its relation to
503 gas-phase precursors during the JULIAC campaign in Germany, *Atmos. Chem. Phys.*, 22, 13137-13152,
504 <https://doi.org/10.5194/acp-22-13137-2022>, 2022.

505 Thaler, R. D., Mielke, L. H., and Osthoff, H. D.: Quantification of nitryl chloride at part per trillion mixing
506 ratios by thermal dissociation cavity ring-down spectroscopy, *Anal. Chem.*, 83, 2761-2766,
507 <https://doi.org/10.1021/ac200055z>, 2011.

508 Tham, Y. J., Wang, Z., Li, Q., Wang, W., Wang, X., Lu, K., Ma, N., Yan, C., Kecorius, S., Wiedensohler, A.,

509 Zhang, Y., and Wang, T.: Heterogeneous N_2O_5 uptake coefficient and production yield of ClNO_2 in polluted
510 northern China: roles of aerosol water content and chemical composition, *Atmos. Chem. Phys.*, 18, 13155-
511 13171, <https://doi.org/10.5194/acp-18-13155-2018>, 2018.

512 Tham, Y. J., Wang, Z., Li, Q., Yun, H., Wang, W., Wang, X., Xue, L., Lu, K., Ma, N., Bohn, B., Li, X.,
513 Kecorius, S., Größ, J., Shao, M., Wiedensohler, A., Zhang, Y., and Wang, T.: Significant concentrations of
514 nitryl chloride sustained in the morning: investigations of the causes and impacts on ozone production in a
515 polluted region of northern China, *Atmos. Chem. Phys.*, 16, 14959-14977, [https://doi.org/10.5194/acp-16-
516 14959-2016](https://doi.org/10.5194/acp-16-14959-2016), 2016.

517 Thornton, J. A., Braban, C. F., and Abbatt, J. P.: N_2O_5 hydrolysis on sub-micron organic aerosols: the effect
518 of relative humidity, particle phase, and particle size, *Phys. Chem. Chem. Phys.*, 5, 4593-4603,
519 <https://doi.org/10.1039/B307498F>, 2003.

520 Thornton, J. A., Kercher, J. P., Riedel, T. P., Wagner, N. L., Cozic, J., Holloway, J. S., Dubé, W. P., Wolfe, G.
521 M., Quinn, P. K., Middlebrook, A. M., Alexander, B., and Brown, S. S.: A large atomic chlorine source
522 inferred from mid-continental reactive nitrogen chemistry, *Nature.*, 464, 271-274,
523 <https://doi.org/10.1038/nature08905>, 2010.

524 Wahner, A., Mentel, T. F., Sohn, M., and Stier, J.: Heterogeneous reaction of N_2O_5 on sodium nitrate aerosol,
525 *J. Geophys. Res. Atmos.*, 103, 31103-31112, <https://doi.org/10.1029/1998JD100022>, 1998.

526 Wang, H., Yuan, B., Zheng, E., Zhang, X., Wang, J., Lu, K., Ye, C., Yang, L., Huang, S., and Hu, W.:
527 Formation and impacts of nitryl chloride in Pearl River Delta, *Atmos. Chem. Phys.*, 22, 14837-14858,
528 <https://doi.org/10.5194/acp-22-14837-2022>, 2022.

529 Wang, H., Wang, H., Lu, X., Lu, K., Zhang, L., Tham, Y. J., Shi, Z., Aikin, K., Fan, S., Brown, S. S., and
530 Zhang, Y.: Increased night-time oxidation over China despite widespread decrease across the globe, *Nat.*
531 *Geosci.*, 16, 217-223, <https://doi.org/10.1038/s41561-022-01122-x>, 2023.

532 Wang, H., Chen, X., Lu, K., Tan, Z., Ma, X., Wu, Z., Li, X., Liu, Y., Shang, D., Wu, Y., Zeng, L., Hu, M.,
533 Schmitt, S., Kiendler-Scharr, A., Wahner, A., and Zhang, Y.: Wintertime N_2O_5 uptake coefficients over the
534 North China Plain, *Sci. Bull.*, 65, 765-774, <https://doi.org/10.1016/j.scib.2020.02.006>, 2020.

535 Wang, T., Tham, Y. J., Xue, L., Li, Q., Zha, Q., Wang, Z., Poon, S. C. N., Dubé, W. P., Blake, D. R., Louie, P.
536 K. K., Luk, C. W. Y., Tsui, W., and Brown, S. S.: Observations of nitryl chloride and modeling its source and
537 effect on ozone in the planetary boundary layer of southern China, *J. Geophys. Res. Atmos.*, 121, 2476-2489,
538 <https://doi.org/10.1002/2015JD024556>, 2016.

539 Xia, M., Peng, X., Wang, W., Yu, C., Wang, Z., Tham, Y. J., Chen, J., Chen, H., Mu, Y., and Zhang, C.:
540 Winter ClNO₂ formation in the region of fresh anthropogenic emissions: seasonal variability and insights
541 into daytime peaks in northern China, *Atmos. Chem. Phys.*, 21, 15985-16000, [https://doi.org/10.5194/acp-](https://doi.org/10.5194/acp-21-15985-2021)
542 [21-15985-2021](https://doi.org/10.5194/acp-21-15985-2021), 2021.

543 Xia, M., Peng, X., Wang, W., Yu, C., Sun, P., Li, Y., Liu, Y. A. H. C. t. A.-P. O. A. C., Xu, Z., Wang, Z., Xu,
544 Z., Nie, W., Ding, A., and Wang, T.: Significant production of ClNO₂ and possible source of Cl₂ from N₂O₅
545 uptake at a suburban site in eastern China, *Atmos. Chem. Phys.*, 20, 6147-6158, [https://doi.org/10.5194/acp-](https://doi.org/10.5194/acp-20-6147-2020)
546 [20-6147-2020](https://doi.org/10.5194/acp-20-6147-2020), 2020.

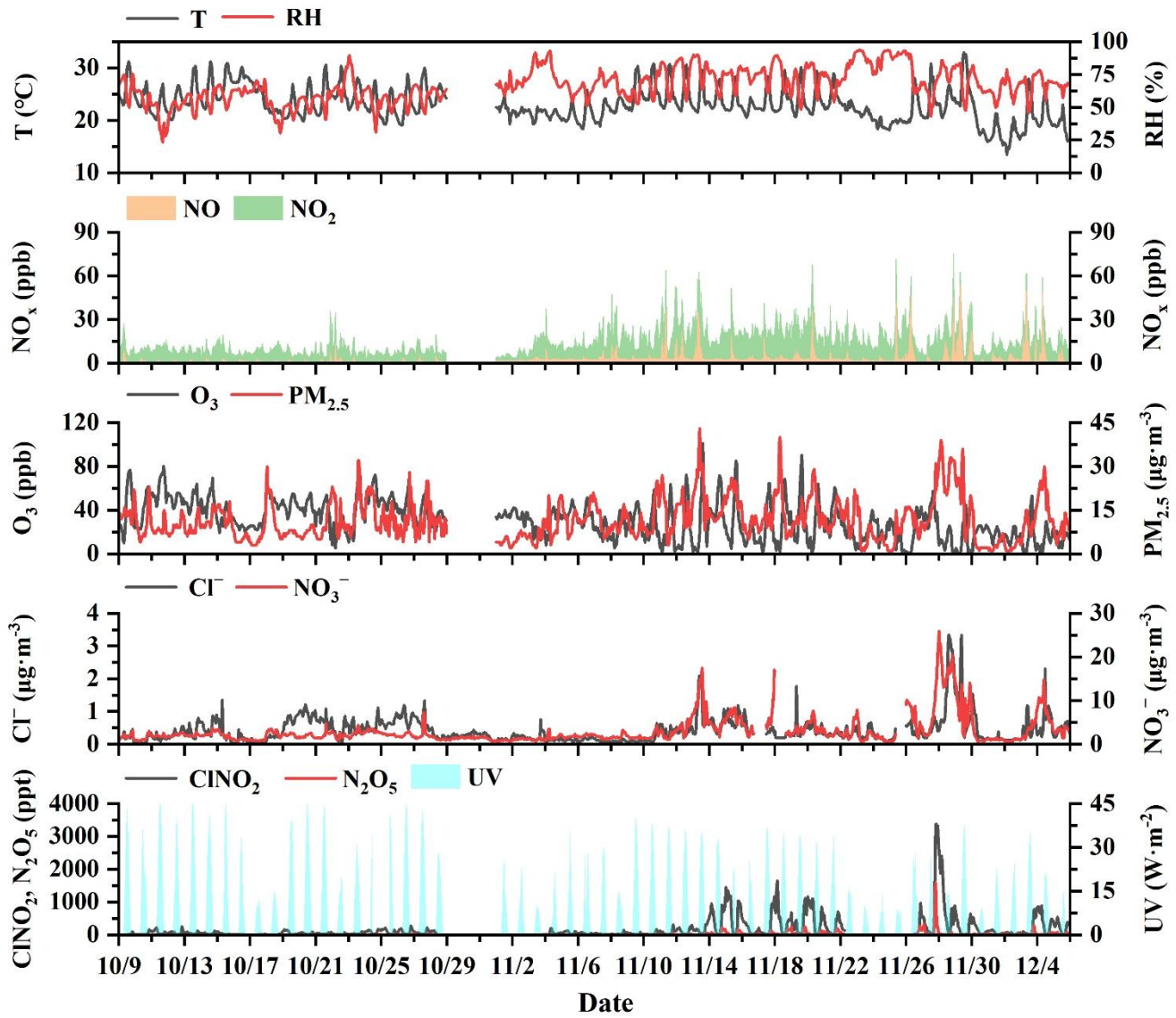
547 Xue, L. K., Saunders, S. M., Wang, T., Gao, R., Wang, X. F., Zhang, Q. Z., and Wang, W. X.: Development
548 of a chlorine chemistry module for the Master Chemical Mechanism, *Geosci. Model Dev.*, 8, 3151-3162,
549 <https://doi.org/10.5194/gmd-8-3151-2015>, 2015.

550 Yan, C., Tham, Y. J., Nie, W., Xia, M., Wang, H., Guo, Y., Ma, W., Zhan, J., Hua, C., and Li, Y.: Increasing
551 contribution of nighttime nitrogen chemistry to wintertime haze formation in Beijing observed during
552 COVID-19 lockdowns, *Nat. Geosci.*, 16, 975-981, <https://doi.org/10.1038/s41561-023-01285-1>, 2023.

553 Yi, X., Sarwar, G., Bian, J., Huang, L., Li, Q., Jiang, S., Liu, H., Wang, Y., Chen, H., and Wang, T.:
554 Significant Impact of Reactive Chlorine on Complex Air Pollution Over the Yangtze River Delta Region,
555 China, *J. Geophys. Res. Atmos.*, 128, e2023JD038898, <https://doi.org/10.1029/2023JD038898>, 2023.

556 Yun, H., Wang, T., Wang, W., Tham, Y. J., Li, Q., Wang, Z., and Poon, S. C. N.: Nighttime NO_x loss and
557 ClNO₂ formation in the residual layer of a polluted region: Insights from field measurements and an iterative
558 box model, *Sci. Total Environ.*, 622-623, 727-734, <https://doi.org/10.1016/j.scitotenv.2017.11.352>, 2018.

559 Zang, H., Zhao, Y., Huo, J., Zhao, Q., Fu, Q., Duan, Y., Shao, J., Huang, C., An, J., Xue, L., Li, Z., Li, C.,
560 and Xiao, H.: High atmospheric oxidation capacity drives wintertime nitrate pollution in the eastern Yangtze
561 River Delta of China, *Atmos. Chem. Phys.*, 22, 4355-4374, <https://doi.org/10.5194/acp-22-4355-2022>, 2022.

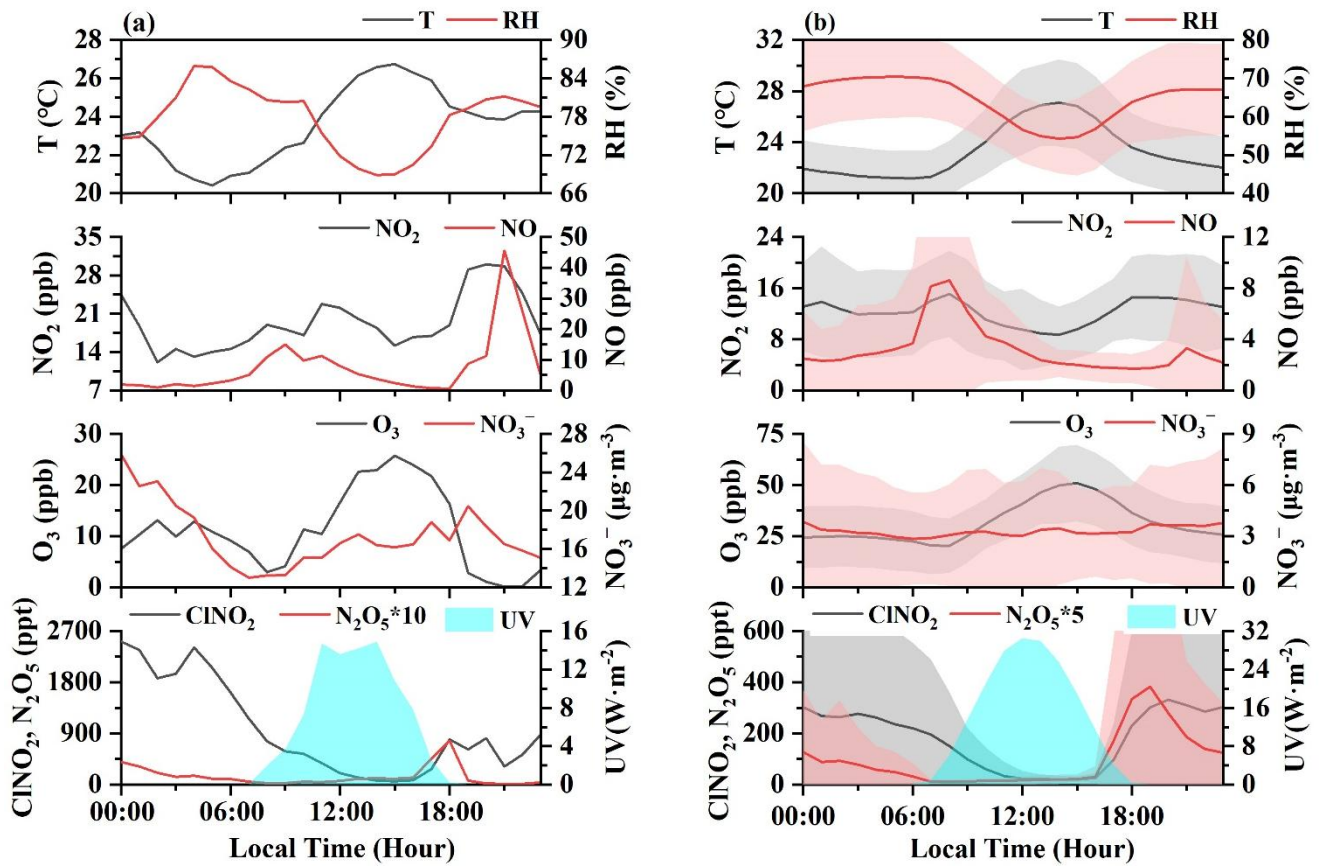


562

563

Figure 1. The time series of CINO₂, related precursors, and meteorological parameters during the autumn observation period.

564



565
 566 Figure 2. Diurnal variations of ClNO₂ and other related parameters for the highest concentrations of ClNO₂
 567 (case) on November 28th (a) and the observation-average condition (from 9 October to 5 December) (b).
 568
 569
 570

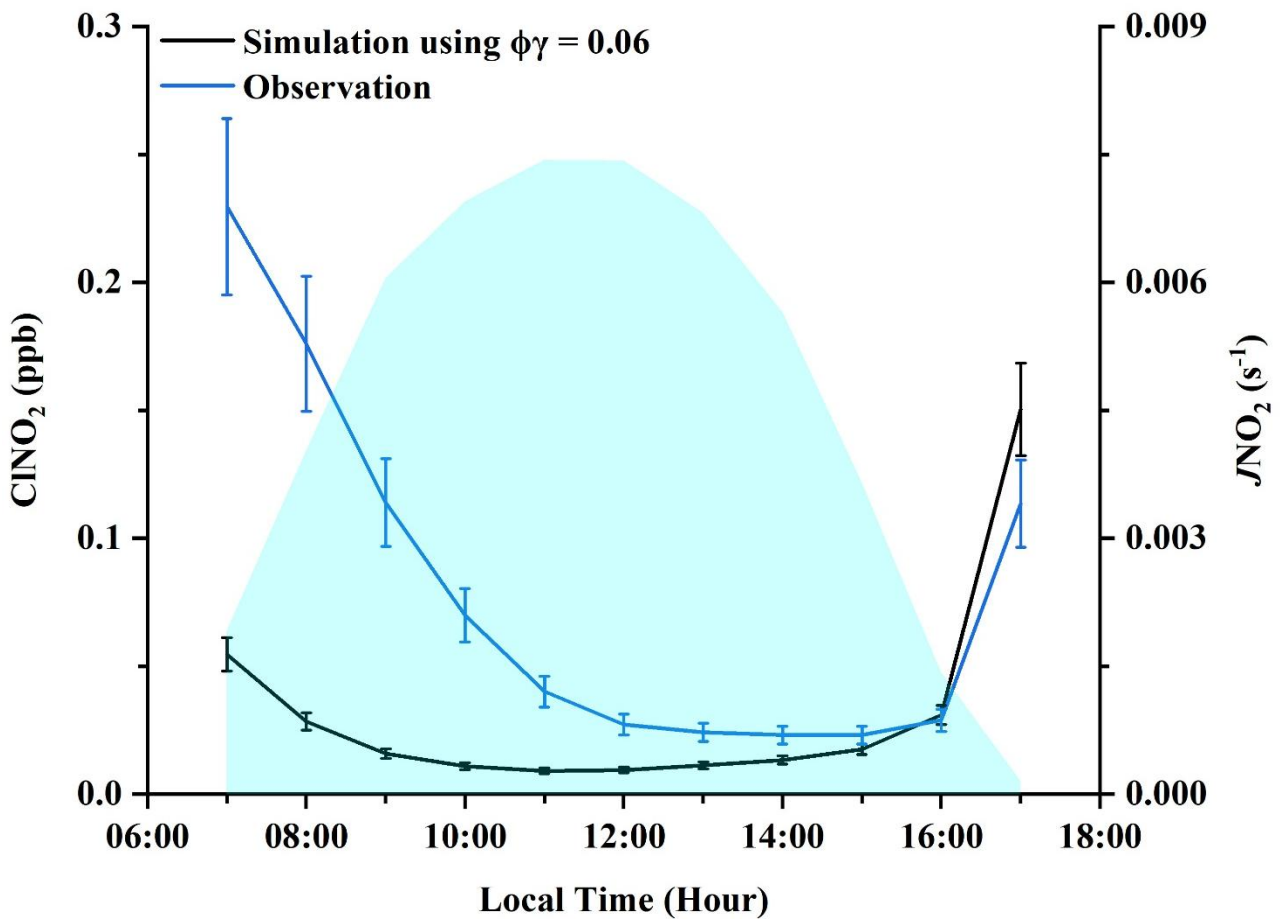
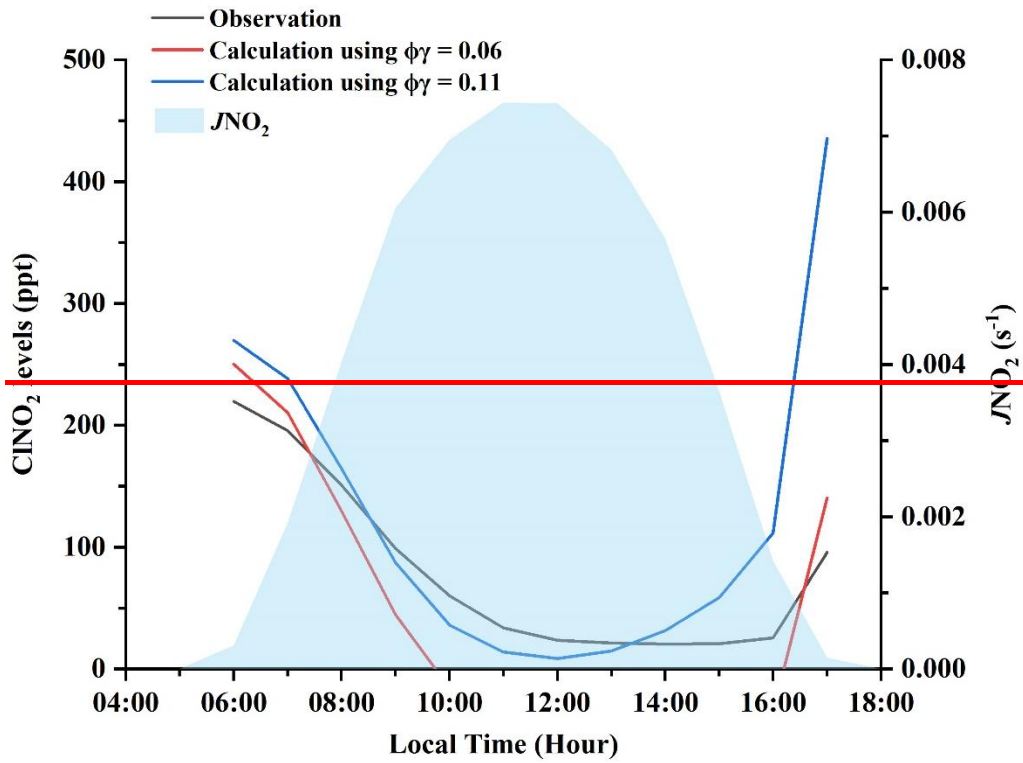
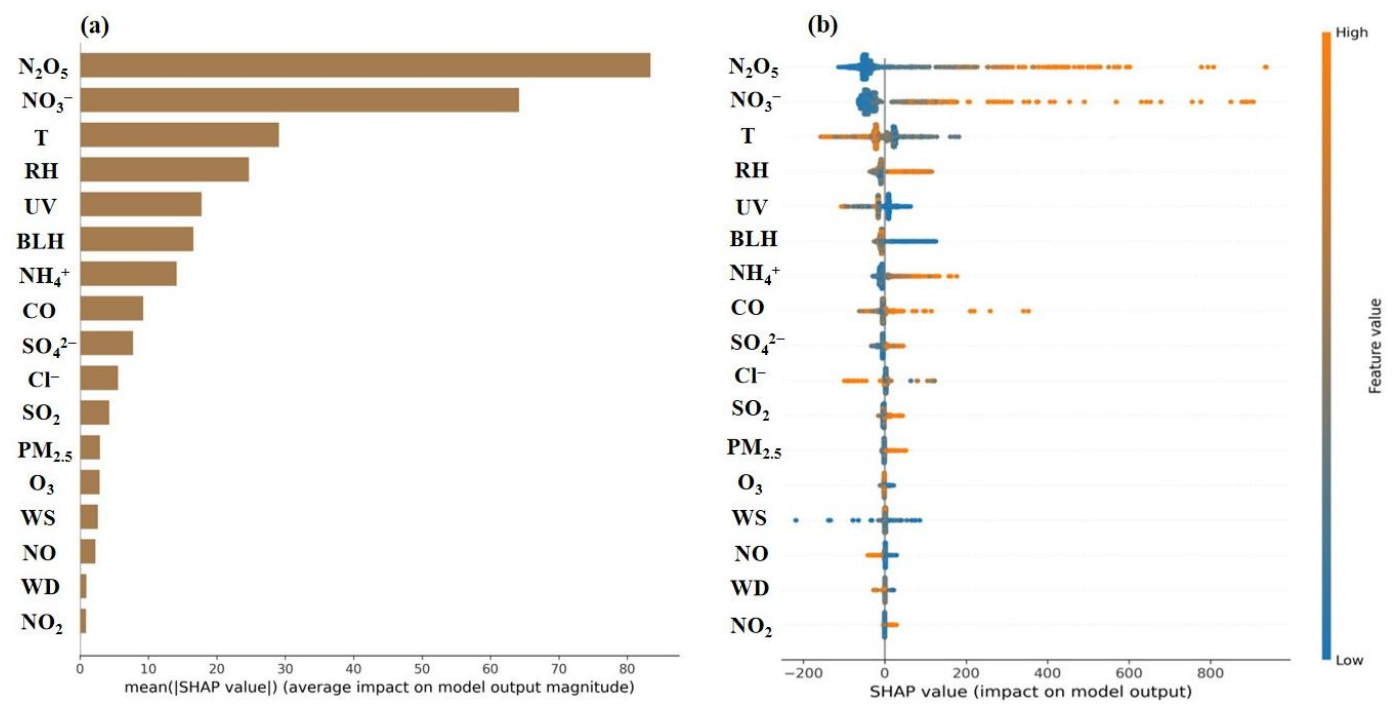


Figure 3. Comparisons of daytime ClNO₂ levels between observation and simulation with a $\phi(\text{ClNO}_2)$ of 1.0 and a $\gamma(\text{N}_2\text{O}_5)$ of 0.06 ($\phi\gamma = 0.06$).

Comparisons of daytime ClNO₂ levels between observation, and calculation using Eq. (4) with a $\phi(\text{ClNO}_2)$

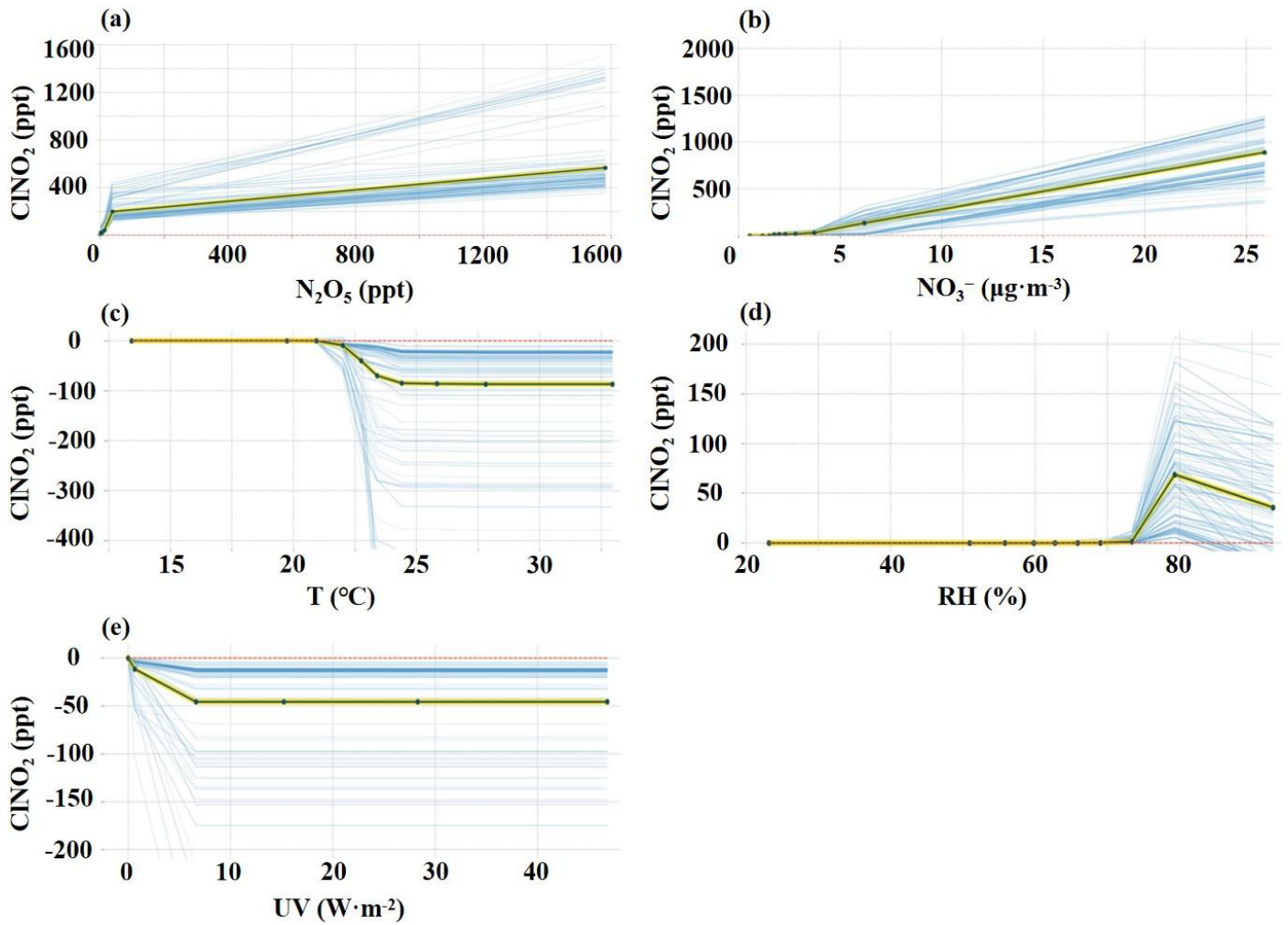
576
577
578

of 1.0 and a $\gamma(\text{N}_2\text{O}_5)$ of 0.06 ($\phi\gamma = 0.06$), or a $\phi(\text{ClNO}_2)$ of 1.0 and a $\gamma(\text{N}_2\text{O}_5)$ of 0.11 ($\phi\gamma = 0.11$).

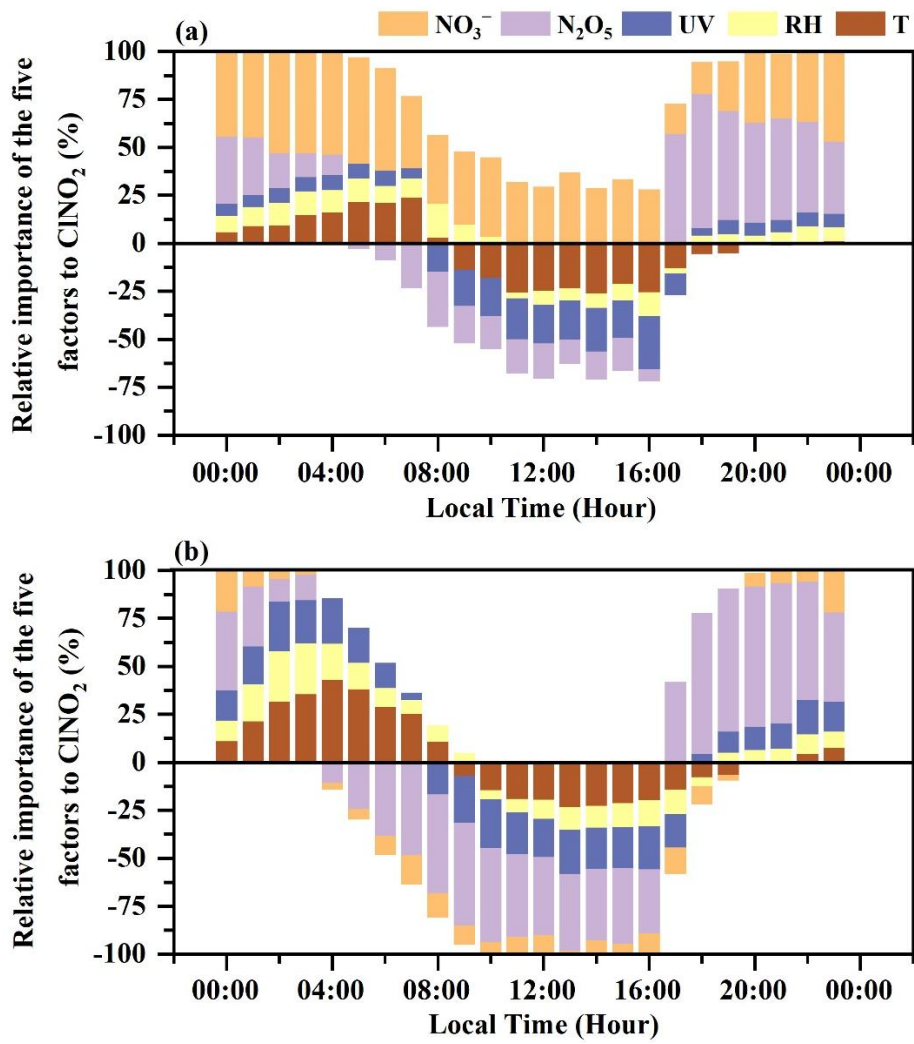


579
580
581

Figure 4. Relative importance of each feature to ClNO_2 using XGBoost-SHAP during the autumn observation period. The mean absolute SHAP value (a), summary plot of SHAP values of each feature (b).



582
 583 Figure 5. Isolation plots of PDP for N₂O₅ (a), NO₃⁻ (b), T (c), RH (d), and UV (e). The average variations of
 584 simulated CINO₂ with factors' changes spline are indicated by the yellow and black curve, and blue curves
 585 presents all situations during the whole observation period.



595

596

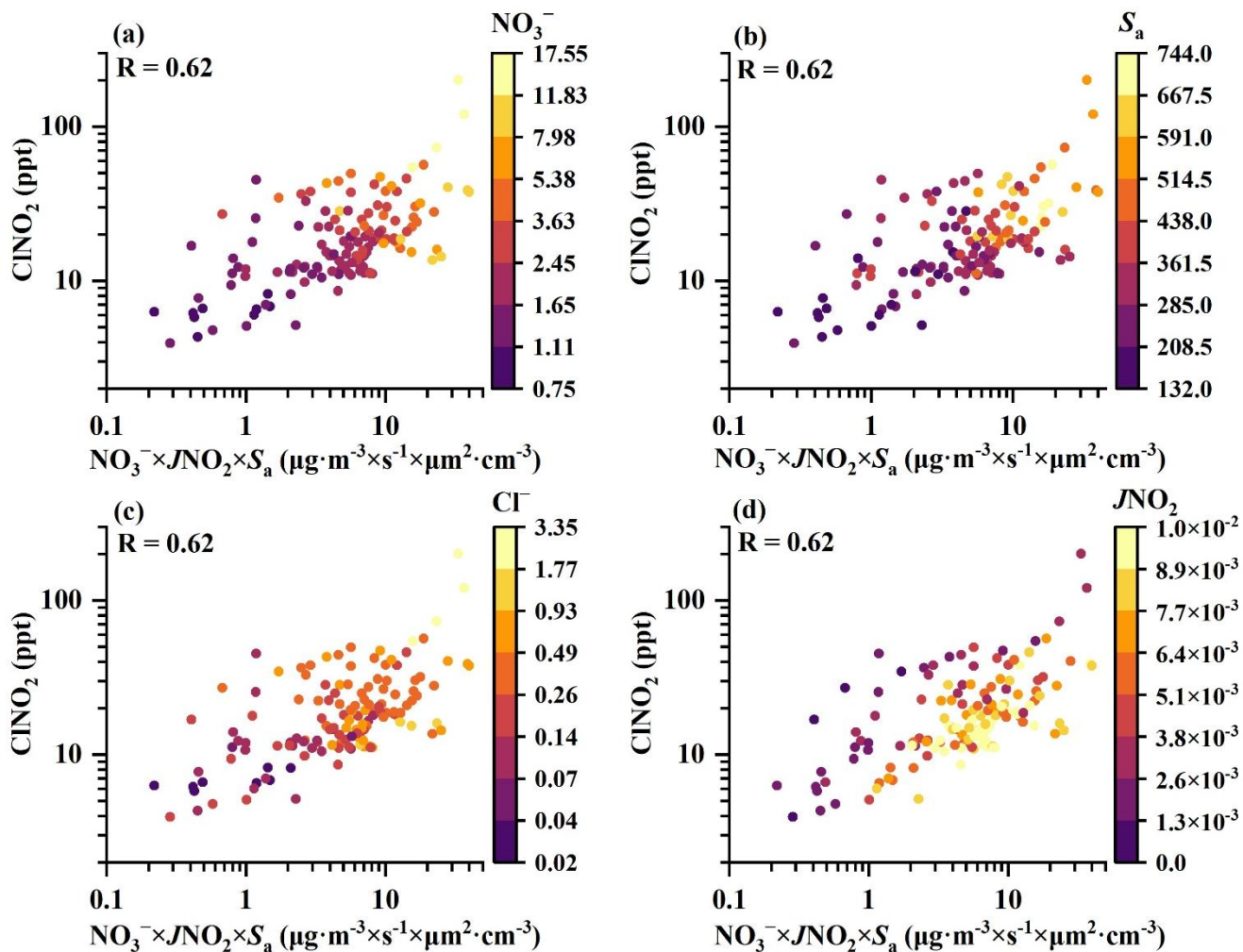
597

598

599

600

Figure 6. The diurnal variations of the relative importance of factors to ClNO₂ based on the SHAP values under the high (> 3.7 µg·m⁻³) (a) and low (< 3.7 µg·m⁻³) (b) ClNO₂ concentrations.



601

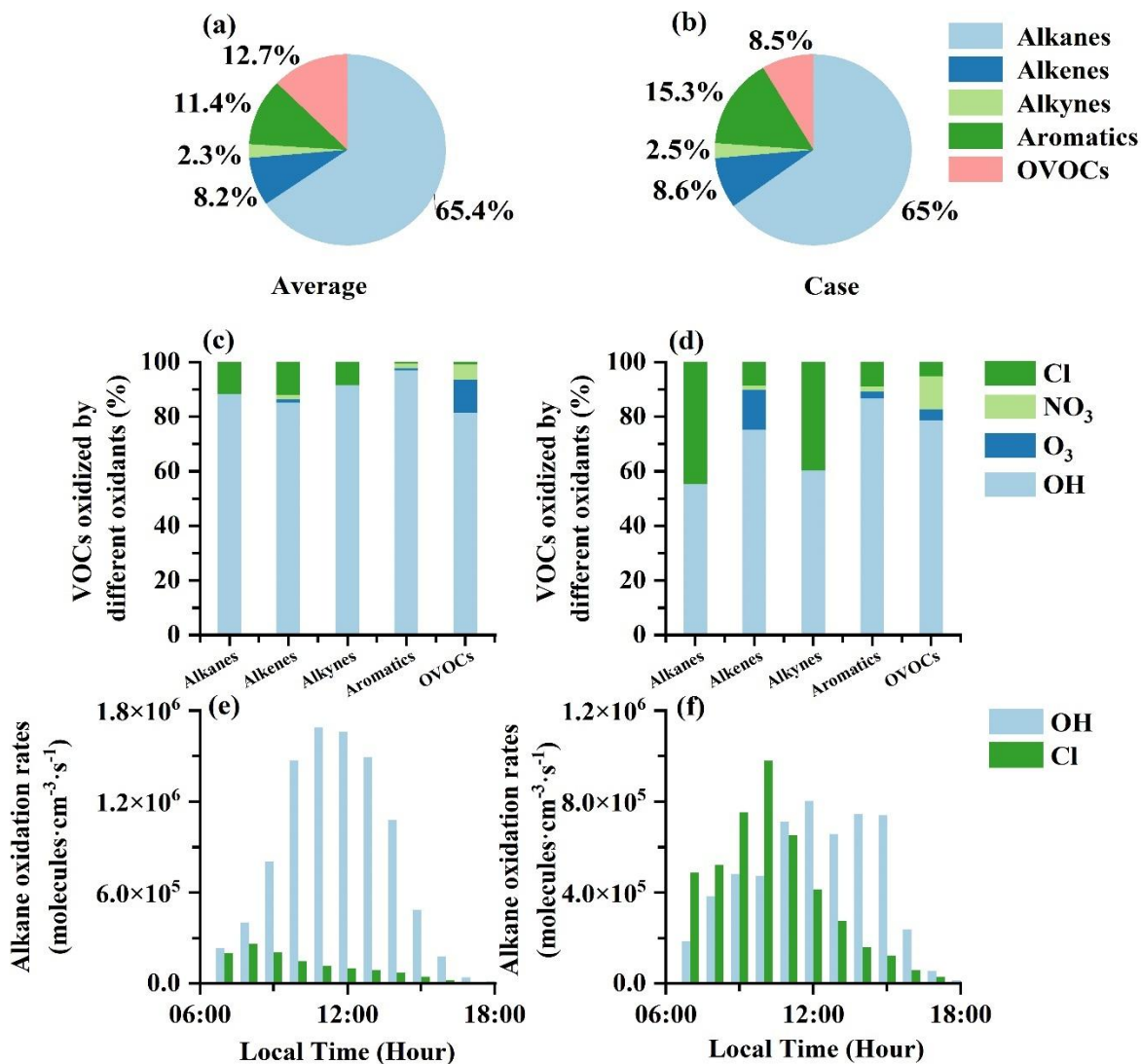
602

603

604

605

Figure 7. The relationship of daytime ClNO_2 concentrations (12:00-15:00 Local Time) and a proxy of nitrate (NO_3^-) photolysis ($\text{NO}_3^- \times J\text{NO}_2 \times S_a$). The color of the dots respects the NO_3^- (a), S_a (b), Cl^- (c), $J\text{NO}_2$ (d), respectively.



606

607

608

609

610

611

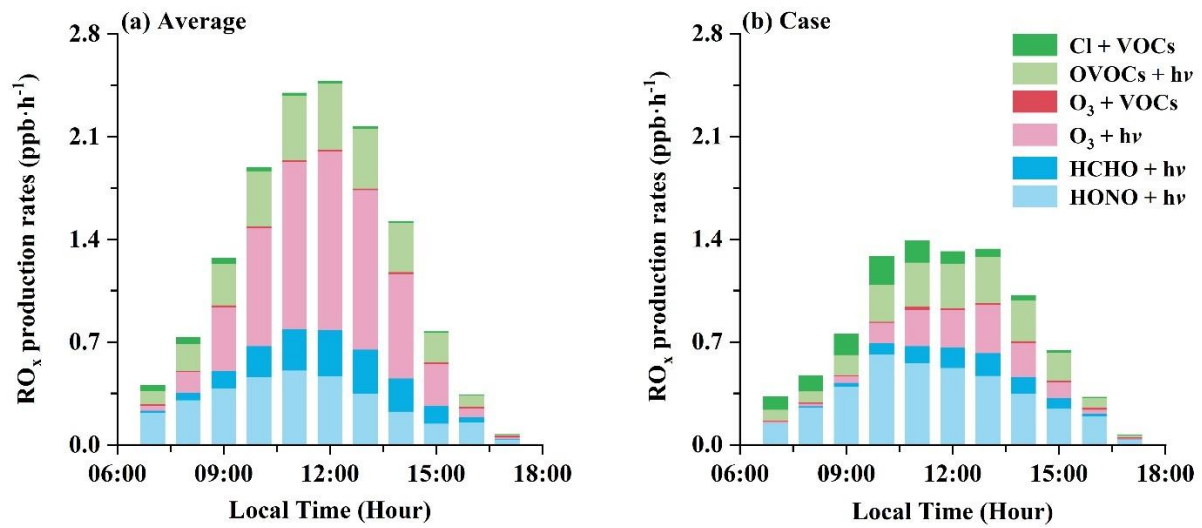
612

613

614

615

Figure 8. The impacts of Cl radicals released by ClNO₂ photolysis and other atmospheric oxidants (including OH, NO₃, and O₃) on VOC oxidation under the observation-average condition and high ClNO₂ case, respectively. The contributions of different VOC groups oxidized by Cl radical during the observation-average (a). The contributions of different VOC groups oxidized by Cl radical during the case (b). The contributions of different atmospheric oxidants (including OH, Cl, NO₃, and O₃) to VOC groups during the observation-average (c). The contributions of different atmospheric oxidants (including OH, Cl, NO₃, and O₃) to VOC groups during the case (d). Comparisons of alkane oxidation rates (molecules·cm⁻³·s⁻¹) by OH and Cl radical during the observation-average (e). Comparisons of alkane oxidation rates by OH and Cl radical (molecules·cm⁻³·s⁻¹) during the case (f).



616
 617 Figure 9. The contributions of different production pathways to RO_x production rates under the observation-
 618 average condition (a) and high $ClNO_2$ case (b), respectively.
 619
 620
 621
 622
 623
 624
 625
 626
 627
 628
 629

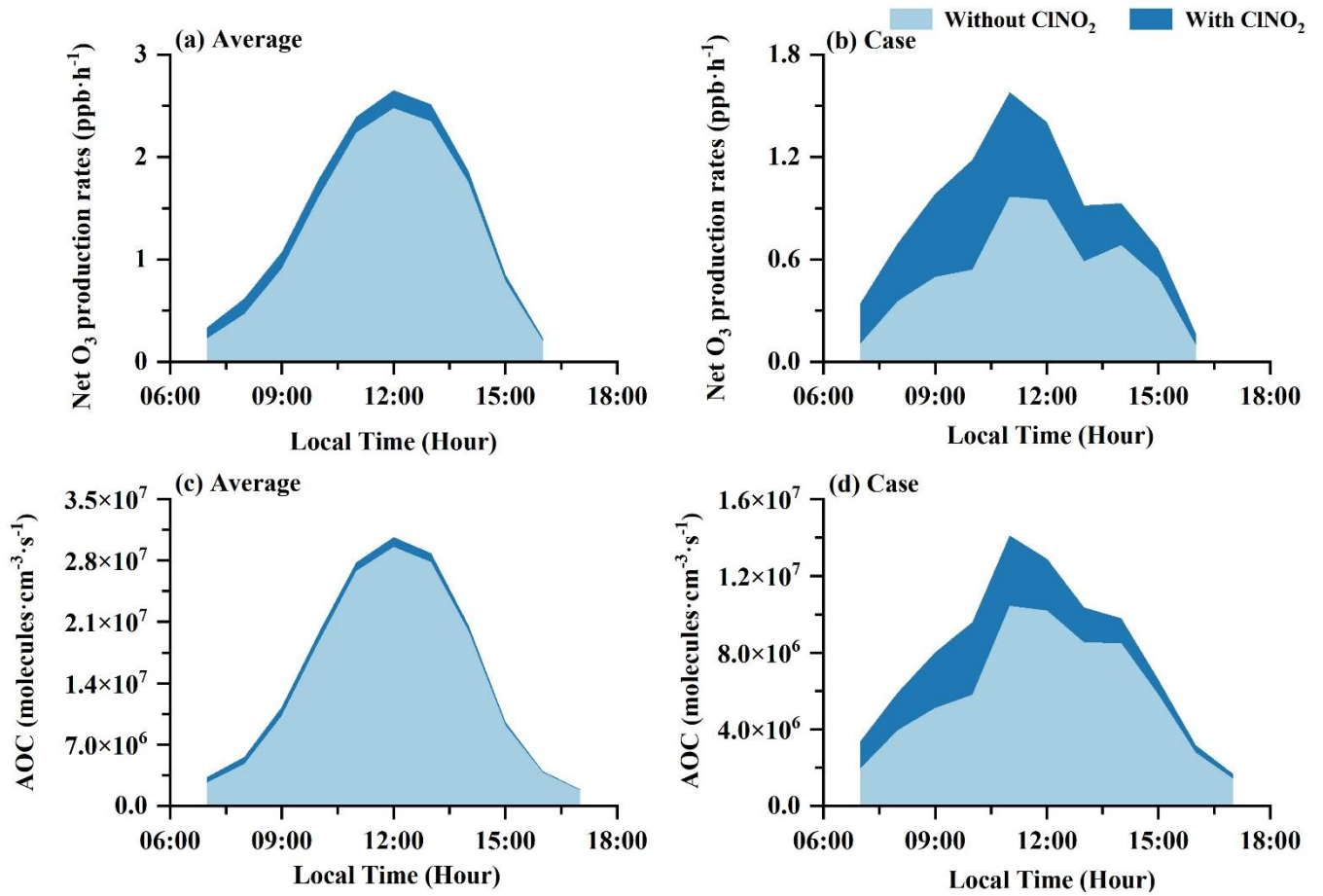


Figure 10. The impacts of Cl radicals released by ClNO₂ photolysis on net O₃ production rates and the AOC levels under the observation-average condition (a, c) and high ClNO₂ case (b, d), respectively.

647 Table 1. Relative importance of Cl, OH, and O₃ to the daytime oxidation of VOC groups (including alkanes,
648 alkenes, alkynes, aromatics, and OVOCs) around the world (Xue et al., 2015; Bannan et al., 2015; Bannan et
649 al., 2017; Rutherford et al., 1995; Fraser et al., 1997).

	Xiamen (average)	Xiamen (case)	Hong Kong (max)	London (average)	Weybourne (average)	Boston	LA
Alkane Cl%	11.7	44.8	53.0	3.5	1.0	8.5	9.9
Alkane OH%	88.3	55.2	47.0	96.5	99.0	91.5	90.1
Alkane O ₃ %	-	-	-	-	-	-	-
Alkene Cl%	12.2	8.7	14.0	0.6	0.4	0.3	0.3
Alkene OH%	85.0	75.2	81.0	77.9	78.3	33	31.3
Alkene O ₃ %	1.2	14.7	5.0	21.5	21.4	66.7	68.4
Alkyne Cl%	8.5	40.0	-	7.0	2.6	8.7	8.7
Alkyne OH%	91.5	60.0	-	91.8	96.7	89.7	89.7
Alkyne O ₃ %	-	-	-	1.2	0.7	1.6	1.6
Aromatics Cl%	0.7	9.1	11.0	-	-	-	-
Aromatics OH%	97.0	86.6	89.0	-	-	-	-
Aromatics O ₃ %	0.7	2.6	-	-	-	-	-
OVOCs Cl%	0.9	5.2	6.0	-	-	-	-
OVOCs OH%	81.4	78.7	85.0	-	-	-	-
OVOCs O ₃ %	12.0	3.9	-	-	-	-	-

650

651

652

653

654

655

656

657

658

659

660

661

662

663

664

665 Table 2. The impacts of ClNO₂ photolysis on RO_x (OH, HO₂, and RO₂) levels, P(RO_x), and P(O₃) around the
 666 world (Xia et al., 2021; Wang et al., 2022; Tham et al., 2016; Wang et al., 2016; Xue et al., 2015; Bannan et
 667 al., 2017; Jeong et al., 2019).

Study Area	Season	OH	HO ₂	RO ₂	P(RO _x)	P(O ₃)
Xiamen (average)	Autumn	3.7%	7.1%	10.3%	4.9%	6.7%
Xiamen (case)	Autumn	17.9%	34.6%	54.3%	23.8%	41.7%
Wangdu/Beijing/Mt. Tai	Winter	15.0%–22.0%	24.0%–31.0%	36.0%–52.0%	1.3%–3.8%	1.3%–6.2%
Heshan	Autumn	1.5%–2.6%	1.9%–4.6%	3.0%–6.8%	< 2.2%	1.0%–4.9%
Wangdu	Summer	-	-	-	10%–30%	3.0%–13.0%
Mt. Tai Mo Shan, Hong Kong	Winter	40.0%–77.0%	53.0%–106.0%	-	-	11.0%–41.0%
Hok Tsui, Hong Kong	Summer	6.6%	12.2%	45.1%	-	10.3%
Weybourne	Spring	5.0%	7.0%	9.0%	-	-
Seoul	Spring	-	-	-	-	1.0%–2.0%

668